Design of Wide Stopband Narrow-Band BPFs Exhibiting Harmonic Suppression

Sh. Amiri [1], N. Khajavi [2], and M. Khajavi [2]

[1] Scientific Member of E.E. Department
Iranian Research Organization for Science and Technology (IROST), Tehran, Iran
amiri@irost.ir

[2] Faculty of E.E. Department of Dezful Branch
Islamic Azad University, Dezful, Iran
N_khajavi89@yahoo.com, Zefins2011@yahoo.com

Abstract ─ This paper presents narrow-band bandpass filters with wide stopband for WLAN and WiMAX systems. First, open-stub and T-shaped resonators were used to design a filter (F_1) with the center frequency 2.4 GHz. In order to examine the architectures of the proposed resonators, their frequency responses were compared to the response of an LC model. Next, Defected Ground Structure (DGS) was utilized to achieve a wide stopband within the frequency response of F_1. Then, the structure of F_1 (without using DGS) only with some changes in the dimensions of the resonators was employed to design the narrow-band filters F_2 and F_3 with the center frequencies 3.7 GHz and 5.1 GHz, respectively. Advantages of these filters include simplicity, architectural symmetry, tenability for applications at other frequency, and proper bandwidth. The filters also provide optimal return loss and insertion loss.

Index Terms ─ Defected Ground Structure (DGS), narrow-band, open-stub resonators, T-shaped resonators, upper-stopband.

I. INTRODUCTION

High-quality compact bandpass filters are among the common elements in wireless communication systems. Wide-stopband filters are used in nonlinear elements such as power amplifiers or mixers for rejecting noise or unwanted interference in the stopband. Bandpass filters with wide stopbands may be designed for different frequencies. There are different techniques for designing narrow-band filters with wide stopbands. For example, ring resonators have been used to eliminate the second harmonic in a bandpass filter with the center frequency 2.6 GHz. This narrow-band filter, however, does not have an acceptable insertion loss [1]. DGS has been used to improve the filter parameters, including its bandwidth. Dumbbell-Shaped DGS (DS-DGS) was implemented at the ground structure [2]. A bandpass filter with the center frequency 2.4 GHz has been designed by coupling two open-loop DGS slot resonators with microstrip resonators [3]. DGS technique has also been implemented on bandpass filter structures to examine how this technique impacts the results [4]. An LC model has been developed for microstrip lines [5,6].

This paper presents narrow-band bandpass filters with wide stopbands for WLAN and WiMAX applications. Open-stub and T-shaped resonators were used to design the architecture of the filters. The frequency responses of these structures were compared to the frequency response of the LC model in order to examine the architecture of the proposed resonators. For the first filter (F_1) with the center frequency 2.4 GHz, DGS was applied to improve the width of the stopband. Next, it has been shown that due the simplicity and symmetry in the architecture of this filter, two other filters with the center frequencies 3.7 GHz and 5.1 GHz can be constructed only by modifying the dimensions of the resonators.

Submitted On: February 27, 2014
Accepted On: September 6, 2014

II. DESIGNING FILTER F_1

Open-stub resonators and a combination of these resonators with T-shaped resonators were used in designing F_1, and then the stopband of this filter was extended using DGS.

A. Designing open-stubs resonators

The conductive pattern shown in Fig. 1 was employed in designing the proposed resonator. Using open-stub resonators placed in parallel to each other (the resonators are connected through a middle stub), the basic resonator architecture shown in Fig. 2 (a) was obtained.

As seen in the frequency response of the basic resonator (Fig. 2 (b)), this architecture has a resonance frequency of 2 GHz, an insertion loss of -0.22 dB, and a return loss of -32.88 dB. The presence of a neutral harmonic at 5.46 GHz limits the stopband. In addition, the center frequency of this architecture does not match the WLAN frequency. The dimensions of the basic resonator are: L1=5.3 mm, W1=0.1 mm, L2=6.4 mm, W2=0.1 mm, L3=20.06 mm, W3=0.1 mm and G1=0.15 mm.

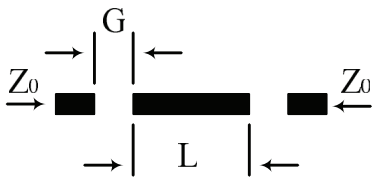

Fig. 1. The conductive pattern.

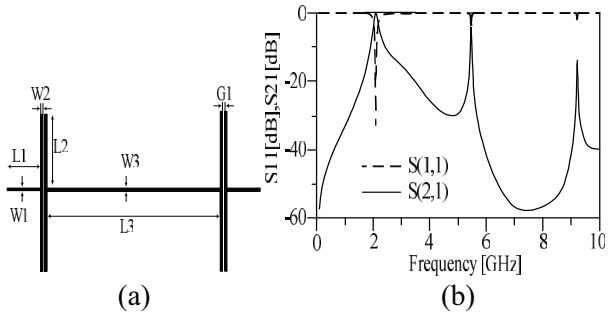

Fig. 2. (a) Basic structure of the proposed resonator, and (b) frequency response of basic structure of the proposed resonator.

B. Analysis of proposed resonator circuit

Before going into the circuit analysis for the proposed resonator, it is quite useful to understand how this resonator functions in terms of wave reflections. The proposed resonator depicted in Fig. 2 (a) uses a capacitor-coupled bipolar stripline resonator. The gap width G1 was selected based on the required capacitance in series connection. The capacitance Cg1 was selected so that a large reactance (X_C) is provided within the frequency range of interest. Larger values of X_C lead to narrower-band filters. Since this reactance is connected in series, large values of X_C create large wave reflections. Overall reflection resulting from such a capacitor coupling depends on the spacing between the capacitors. The proposed bandpass resonator shown in Fig. 2 (a) was designed as follows. For the resonance frequency 2 GHz and the bandwidth 3 dB (167 MHz), the calculated value for Q_L (equation (2)) is 11.976, and using Fig. 3 the value of $\overline{X}_{cr}$ is about 4. Equation (1) can be used to obtain the exact value of $\overline{X}_{cr}$ [7]:

$$Q_L = \frac{\overline{X}_{Cr}}{4}\sqrt{\overline{X}_{Cr}^2+4}\left(\Pi - \arctan\frac{2}{\overline{X}_{Cr}^2}\right). \quad (1)$$

For a filter with the resonance frequency f_0 and the bandwidth BW, Q_L can be obtained using:

$$Q_L = \frac{f_o}{BW}. \quad (2)$$

Equation (3) was used to calculate ϕ_r, the electrical length of the transmission line L_3:

$$\phi_r = \Pi - \arctan\left(\frac{2}{\overline{X}_{Cr}}\right). \quad (3)$$

The value obtained for the electrical length of the transmission line L_3 is $\varphi_r = 153.435^\circ$.

According to equation (4), condition for zero fall is fallowing:

$$2\cos\varphi_r = -\overline{X}_{cr}\sin\varphi_r. \quad (4)$$

According to the values obtained for $\overline{X}_{cr}$ and ϕ_r, 4 draws the relationship is established. Since $\overline{X}_c \approx \overline{X}_{cr}$ is in the frequency range of interest for narrow band frequency characteristics, the value for $\overline{X}_c$ is 4. Using equation (5) and the value of Z_0=50 Ω, the calculated value for the reactance (X_C) is 200 Ω:

$$\overline{X_C} = \frac{X_C}{Z_0}. \quad (5)$$

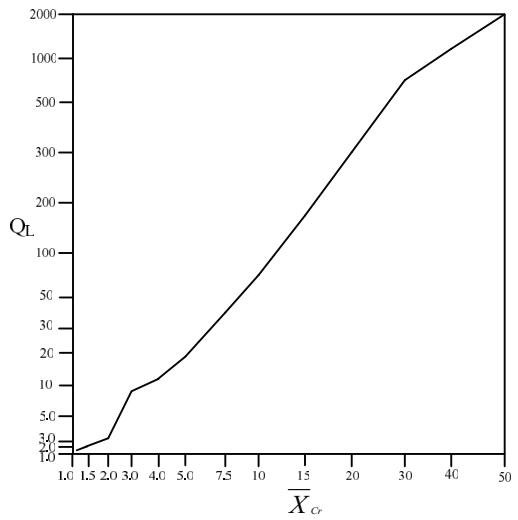

Fig. 3. Q_L was evaluated as a function of $\overline{X}_{cr}$ bandpass filters [7].

C. Designing model LC proposed resonator

The conductive pattern shown in Fig. 4 was used to obtain an equivalent circuit for the transmission line. Equivalent circuit for the transmission line of the conductive pattern is presented to further examine the basic resonator.

Fig. 4. Equivalent circuit for the transmission line of the conductive pattern.

The effective dielectric constant ε_{ref} and characteristic impedance Z_C are used to identify the characteristics of microstrip lines [8]. For substrate R04003 with the thickness H=0.508 mm and a microstrip line with the width W (the width of microstrip lines are presented in Fig. 2), ε_{ref} can be obtained from (6) [7]:

$$\begin{aligned} \varepsilon_{ref} &= \frac{\varepsilon_r+1}{2} + \left\{1+12\left(\frac{H}{W}\right)^{-0.5} + 0.04\left(1-\frac{W}{H}\right)^2\right\} & \frac{W}{H} \le 1 \\ \varepsilon_{ref} &= \frac{\varepsilon_r+1}{2} + \frac{\varepsilon_r-1}{2}\left(1+12\frac{H}{W}\right)^{-0.5} & \frac{W}{H} \ge 1 \end{aligned}. \quad (6)$$

Equation (7) is used to calculate C_a [7]. ε_r is the dielectric constant of free space. C_a is capacitance per unit length for an air substrate:

$$\begin{aligned} C_a &= \frac{2\pi\varepsilon_r}{Ln\left(\frac{8H}{W}+\frac{W}{4H}\right)} & \frac{W}{H} \le 1 \\ C_a &= \varepsilon_r\left(\frac{W}{H}+1.393+0.66Ln\left(\frac{W}{H}+1.444\right)\right) & \frac{W}{H} \ge 1 \end{aligned}. \quad (7)$$

L and C are derived from (8). For this purpose, one should first calculate Phase velocity V_P and characteristic impedance Z_C ($c \simeq 3.0\times10^8$ m/s):

$$Z_C = \frac{120\pi}{\frac{C_a}{\varepsilon_r}\sqrt{\varepsilon_{ref}}}, \quad V_P = \frac{c}{\sqrt{\varepsilon_{ref}}},$$

and

$$L = \frac{Z_C l}{V_P}, \quad C = \frac{l}{Z_C V_P}. \quad (8)$$

In this model (Fig. 5 (a)), Lt1 represents the stubs which connect the ports to the basic resonator, while Lt2 shows the stub connecting open-stub resonators. The gap between the open-stub resonators is denoted by Cg1. The grounded capacitor Cop and the inductor Lop were used to model the open-stub resonators. The LC model is shown in Fig. 5 (a).

Comparison of the frequency response of the LC circuit with the simulation results indicates a proper match between the center frequencies of both frequency responses shown in Fig. 5 (b). The values of inductance and capacitance for the LC model are: Lt1=3 nH, Lt2=8.3 nH, Lop=0.95 nH, Cop=0.5 pF and Cg1=0.37 pF. Table 1 presents the relationships between Cg1, the LC model, the gap between the two open-stub resonators, and the parameters of the frequency response of F_1. Cg1 decreases as G1 increases. This shows an inverse relationship between the resonator gap and its equivalent capacitance. The center frequency shifts toward higher frequencies and return and insertion losses become smaller, which is not optimum.

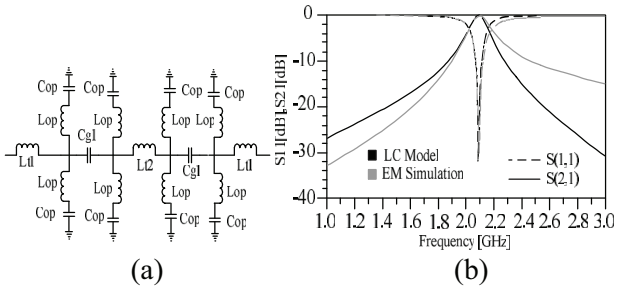

Fig. 5. (a) The LC model of the basic structure, and (b) frequency response of the LC model and EM simulation of the basic structure.

Table 1: The relationship between gap of the two open-stub resonators with LC parameters, and the parameters of the frequency response

Filter F_1	G1=0.15 mm	G1=0.17 mm	G1=0.19 mm	G1=0.21 mm	G1=0.23 mm
Cg1	0.37 pF	0.33 pF	0.31 pF	0.29 pF	0.27 pF
F_0	2 GHz	2.11 GHz	2.12 GHz	2.13 GHz	2.14 GHz
S_{21}	-0.22 dB	-0.24 dB	-0.27 dB	-0.3 dB	-0.34 dB
S_{11}	-32.88 dB	-30.7 dB	-29.97 dB	-28.35 dB	-27.3 dB

D. Designing model T-shape resonators

In the next step, T-shaped resonators were used to improve the stopband and to obtain a center frequency which is consistent with IEEE 802.11a (Fig. 6 (a)).

The arrangement of the T-shaped resonators has created a deep zero at 5.4 GHz. Frequency response of T-shape structure resonators is shown in Fig. 6 (b). The dimensions of the T-shaped resonators are: W4=0.247 mm, L4=10.266 mm, W5=1.08 mm, L5=5.74 mm, W6=0.70 mm, L6=1.98 mm and G2=0.24 mm.

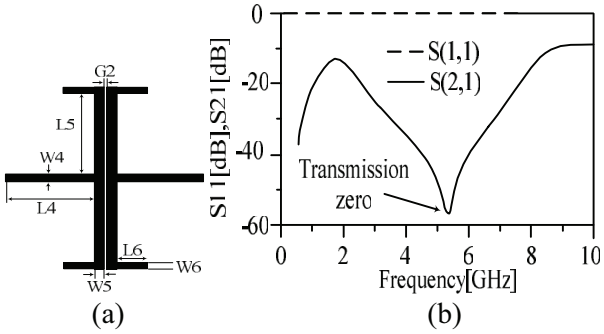

Fig. 6. (a) T-shape structure resonators, and (b) frequency response of T-shape structure resonators.

E. Designing model LC T-shape resonators

Again, an LC model was used to examine these T-shaped resonators. In this model, the microstrip lines are modeled based on their corresponding indices using inductors and capacitors. Cg2 represents the gap between the T-shaped resonators. The open-ended sections are grounded through a capacitor and the transmission lines are modeled by inductors. The model is shown in Fig. 7 (a).

The values of the capacitance and inductance are: L4=0.85 nH, L5=1.45 nH, L6=0.5 nH, C6=0.5 pF and Cg2=0.1 pF. A comparison of the frequency response of the LC model for the T-shaped resonators and the associated EM simulation indicates a good match between the two simulations as seen in Fig. 7 (b).

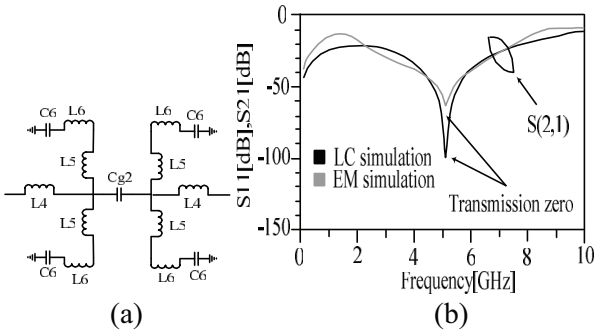

Fig. 7. (a) The LC model of the T-shape structure resonators, and (b) frequency response of the LC model and EM simulation of the T-shape structure resonators.

F. Coupling between two resonators

The presence of a deep zero at 5.4 GHz along with a frequency response with a pole at the same frequency cancels the effect of the zero and the pole at this frequency, thereby widening the stopband. This can be seen in Fig. 8. This results in a center frequency of 2.69 GHz, an insertion loss of -4.36 dB, and a return loss of -2.5 dB, which show a considerable drop in losses compared to the frequency response obtained for open-stub resonators.

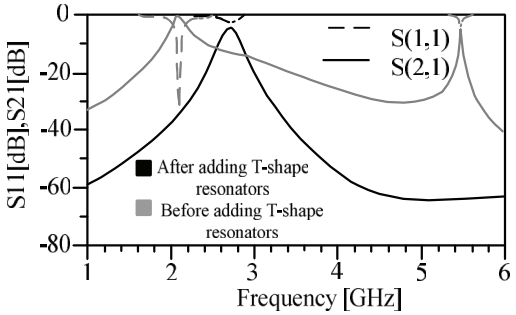

Fig. 8. Comparison of frequency basic structure before and after adding the T-shaped resonators.

In fact, the final architecture of filter F_1 was obtained by putting together the open-stub

resonators and the T-shaped resonators. The architecture is shown in Fig. 9 (a).

Desirable center frequency, insertion loss, return loss, and bandwidth were achieved by changing the dimensions of different parts of the open-stub and T-shaped resonators. The dimensions of the filter structure F_1 are: W1=0.1 mm, L1=3.06 mm, W2=0.34 mm, L2=6.50 mm, W3=0.1 mm, L3=1.35 mm, W4=0.24 mm, L4=10.26 mm, W5=1.08 mm, L5=5.74 mm, W6=0.70 mm, L6=1.98 mm, G2=0.24 mm and G1=0.18 mm. As seen in the frequency response of F_1 (Fig. 9 (b)), return loss and insertion loss for this filter are 32.8 dB and -0.5 dB, respectively. In addition, the bandwidth of F_1 is 112 MHz. Another property of F_1 examined here is sharpness. The value of this parameter is 0.121 GHz. This low sharpness indicates that the frequency response is close to the desirable response. Figure 10 shows a schematic of constructed filter and a comparison of its frequency response to that of the simulation model. As seen in Fig. 10, the two responses are in close agreement. All simulations in this paper were implemented using Momentum simulator in ADS.

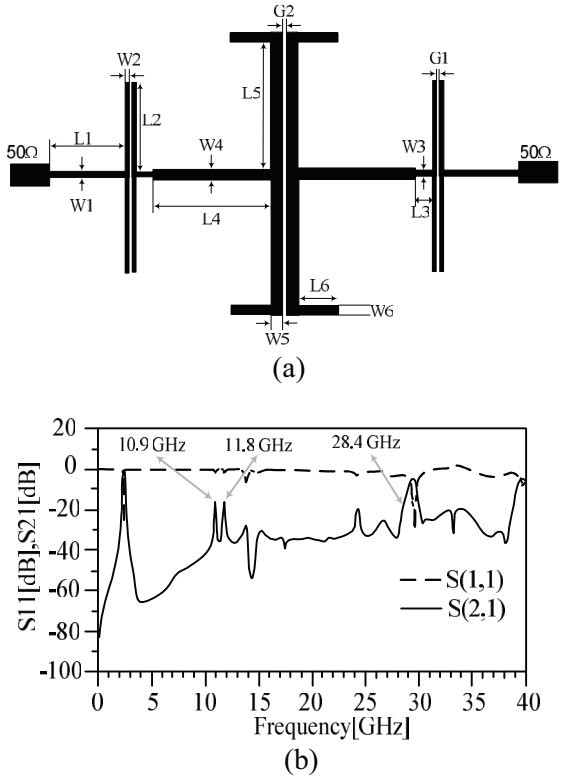

Fig. 9. (a) Structure of the filter F_1, and (b) frequency response of structure of the filter F_1.

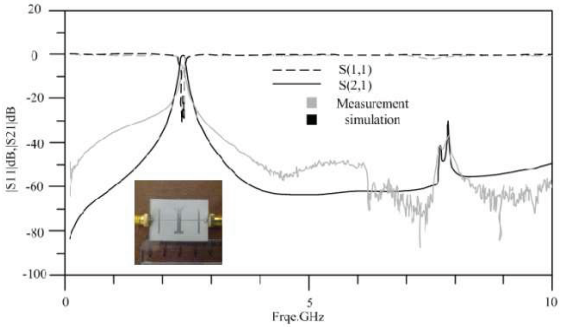

Fig. 10. Comparison of the results EM-simulation and measurement for filter F_1.

G. Adding DGS to structure of the filter F_1

The presence of some harmonics at 10.9 GHz, 11.8 GHz, and 28.4 GHz in the frequency response of filter F_1 has limited the stopband. DGS was used to eliminate the neutral harmonics in the stopband and to widen this band. DGS technique was employed to create the dumbbell-shaped structure shown in Fig. 11. In Fig. 11 (a), the architecture is seen from above. Then in Fig. 11 (b), the substrate and dumbbell-shaped structure is seen from below. Figure 12 shown, compares the frequency responses of filter F_1 before and after applying DGS. Applying DGS shifts all the neutral harmonics in the stopband, up to the frequency 39 GHz, into the levels below -20 dB, thereby widening the stopband by 16.25 F_0.

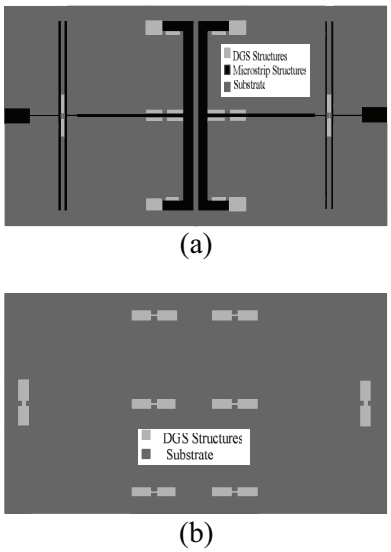

Fig. 11. (a) The architecture seen from above, and (b) the substrate and dumbbell-shaped structure seen from below.

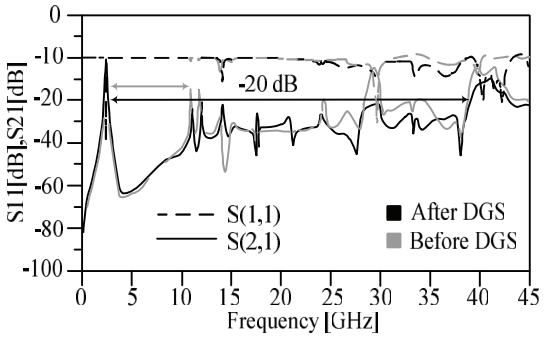

Fig. 12. Compares the frequency responses of filter F_1 before and after applying DGS.

According to the comparison presented in Table 2, DGS improves not only the stopband but also return loss and insertion loss.

Table 2: Comparison of the results for filter F_1 before and after applying DGS

Filter F_1	Center Frequency	Upper-Stop Band	Band Width	Return Loss (dB)	Insertion Loss (dB)
Before DGS	2.42 GHz	12 F_0	0.121 GHz	-33.35	-0.521
After DGS	2.42 GHz	16.25 F_0	0.121 GHz	-38.3	-0.426

III. DESINING FILTER WITH CENTER FREQUENCY 3.7 GHz AND 5.1 GHz

One objective in designing microstrip filters is to design small size architectures with high capabilities which are regarded as advantages of this type of architecture. These small and highly capable architectures can be designed by combining open-stub resonators with T-shaped resonators. Therefore, filter F_2 with the center frequency 3.7 GHz and filter F_3 with the center frequency 5.1 GHz were obtained simply by changing the dimensions of filter F_1. Filters F_1 and F_3 can be used in WLAN applications, while filter F_2 is suitable for WiMAX systems.

A. Designing filter F_2

The architecture of this filter is the same as the architecture of filter F_1, therefore its dimensions are: W1=0.1 mm, L1=5.3 mm, W2=0.16 mm, L2=6.4 mm, W3=0.1 mm, L3=0.5 mm, W4=0.8 mm, L4=8.88 mm, W5=0.8 mm, L5=5.4 mm, W6=0.4 mm, L6=1.6 mm, G1=0.2 mm and G2=0.15 mm. The frequency response of the filter is shown in Fig. 13. As seen in this figure, filter F_2 has its center frequency at 3.7 GHz, a bandwidth of 214 MHz, an insertion loss of -0.42 dB and a return loss of -41.578 dB. Since S_{21} is below -20 dB, for frequencies up to 11.79 GHz, the second and third harmonics are eliminated in filter F_2.

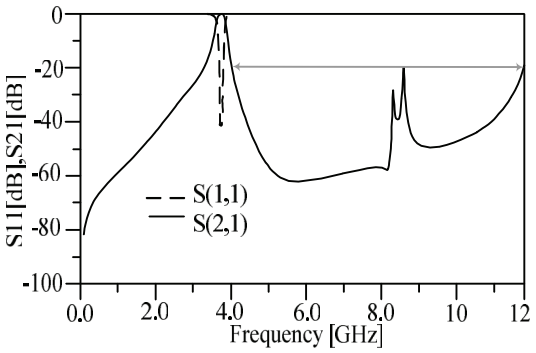

Fig. 13. Frequency response of the filter F_2.

B. Designing filter F_3

The architecture of this filter is the same as the architecture of filter F_1, therefore its dimensions are: W1=0.1 mm, L1=4.69 mm, W2=0.12 mm, L2=4.48 mm, W3=0.1 mm, L3=0.76 mm, W4=0.56 mm, L4=6.16 mm, W5=0.616 mm, L5=3.66 mm, W6=0.397 mm, L6=1.12 mm, G1=0.14 mm and G2=0.105 mm.

The frequency response of this filter is shown in Fig. 14. As seen in this figure, filter F_3 has its center frequency at 5.1 GHz, a bandwidth of 423 MHz, an insertion loss of -0.318 dB and a return loss of -53.23 dB. Since S_{21} is below -20 dB, for frequencies up to 16.27 GHz, the first and second harmonics are eliminated in filter F_3. Table 3 compares the results obtained for the filters designed in this paper.

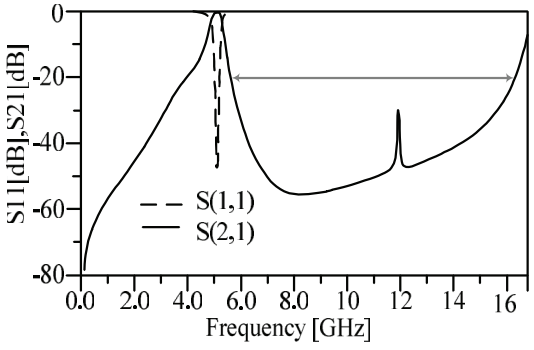

Fig. 14. Frequency response of F_3 filter.

Table 3: Final results for optimized architectures of the proposed microstrip single-band bandpass filters

Filter Name	F_1	F_2	F_3
Center Frequency (GHz)	2.42	3.7	5.1
Insertion Loss (dB)	-0.426	-0.42	-0.318
Return Loss (dB)	-38.3	-41.57	-53.23
Fractional Band Width (GHz)	0.121	0.214	0.423
Upper Stop Band (x F_0)	16.25	3	2
Size of the Filter (mm*mm)	37.182*13.4	36.46*12.91	29.81*9

IV. COUPLING COEFFICIENTS CALCULATED FOR THE THREE FILTERS

Effective coupling between the resonators was evaluated using coupling bandwidth [9]. In calculation of effective coupling for a narrowband filter we have:

$$K = \frac{W_2^2 - W_1^2}{W_2^2 + W_1^2} \approx \frac{W_2 - W_1}{W_0}, \quad (9)$$

$$W_0 = \frac{W_2 + W_1}{2}, \quad (10)$$

$$\Delta W_{12} = W_2 - W_1 = W_0 \times K. \quad (11)$$

Where K represents effective coupling, ΔW_{12} represents coupling bandwidth, and finally W_1 and W_2 are equal to resonator peak frequencies, and W_0 represents the center frequency. Bandwidth of an optimum filter is proportional to ΔW_{12}. The data presented in Table 2 were used in these calculations. Given the center frequencies and bandwidths of the three filters, effective coupling for F_1, F_2, and F_3 is 0.05, 0.057, and 0.082, respectively.

V.CONCLUSION

This paper presents narrow-band bandpass filters with wide stopband for WLAN and WiMAX applications. First, using parallel open-stub resonators connected by stubs, the frequency response of the basic resonator was obtained with the resonance frequency 2 GHz and a pole at 5.4 GHz. T-shaped resonators were placed next to open-stub resonators to cancel this pole, widen the stopband, and construct the final architecture for filter F_1. The T-shaped resonators create a deep zero at the same frequency, thereby cancelling the effect of this pole. To examine the architectures of the proposed resonators, the frequency responses of these architectures were compared with the frequency responses of their corresponding LC model. Then, narrow-band filters with the center frequencies 3.7 GHz and 5.1 GHz (for filter F_2 and filter F_3, respectively) were obtained simply by changing the dimensions of the resonators in the basic structure of filter F_1. Finally, DGS was utilized to achieve a wide stopband in the frequency response of filter F_1. An advantage of these filters is having a good bandwidth. In addition, these filters have optimal return loss and insertion loss.

REFERENCES

[1] J. Fraresso and C. E. Saavedra, "Narrowband bandpass filter exhibiting harmonic suppression," *Electronics Letters*, vol. 39, no. 16, pp. 1189-1190, 2003.

[2] A. Kumar and M. V. Kartikeyan, "A design of microstrip bandpass filter with narrow bandwidth using DGS/DMS for WLAN," *2013 National Conference on Communications (NCC)*, New Delhi, India, pp. 1-4, 2013.

[3] P. Vagner and M. Kasal, "A novel bandpass filter using a combination of open-loop defected ground structure and half-wavelength microstrip resonators," *Radioengineering*, vol. 19, no. 3, pp. 392-396, 2010.

[4] M. Kufa and Z. Raida, "Comparison of planar fractal filters on defected ground substrate," *Radioengineering*, vol. 21, no. 4, pp. 1019-1024, 2012.

[5] M. Shobeyri and M. H. Vadjed Samiei, "Compact ultra-wideband bandpass filter with defected ground structure," *Progress In Electromagnetics Research Letters*, vol. 4, pp. 25-31, 2008.

[6] T. Yang, M. Tamura, and T. Itoh, "Compact hybrid resonator with series and shunt resonances used in miniaturized filters and balun filters," *IEEE Transactions on Microwave Theory and Techniques*, vol. 58, no. 2, pp. 390-402, 2010.

[7] P. A. Rizzi, "Microwave engineering: passive circuits," Book, *Prentice Hall PTR*, 1988.

[8] J. S. Hong and M. J. Lancaster, "Microstrip filters for RF/microwave applications," *Book* (Hong, et al., 2001), A Wiley-Interscience Publication, *John Wily & Sons, Inc*., 2001.

[9] A. C. Guyette, "Alternative architectures for

narrowband varactor-tuned bandpass filters," *Proceedings of the 4th European Microwave Integrated Circuits Conference*, Rome, Italy, pp. 28-29, September 2009.

Shervin Amiri is a Scientific Member of the Electrical Engineering Department of Iranian Research Organization for Science and Technology (IROST) in Tehran, I.R. Iran. He received the Associate Professor degree in 2013. His research interest fields are Antenna and RF subsystems in microwave and millimeter wave bands.

Nafiseh Khajavi received the M.Sc. degree in Electrical Engineering from Kermanshah Science and Research Branch Islamic Azad University, Kermanshah. Her research interests include microstrip filter, the analysis and design of high-frequency electronics and microwave passive circuits.

Mahboubeh Khajavi received the M.Sc. degree in Electrical Engineering from South of Tehran Branch Islamic Azad University. Her research interests include microstrip filter, the analysis and design of high-frequency electronics.